

Thermal Reduction of Graphite Oxide Derivatives for Preparation of Supports for Platinum Hydrogenation Catalysts

S. D. Kushch^{a*}, N. S. Kuyunko^a, A. A. Arbuzov^a, L. A. Korshunova^a, and G. V. Bondarenko^b

^a Institute of Problems of Chemical Physics, Russian Academy of Sciences,
pr. Akademika Semenov 1, Chernogolovka, 142432 Russia

*e-mail: ksd@icp.ac.ru

^b Institute of Experimental Mineralogy, Russian Academy of Sciences, Chernogolovka, Russia

Received February 15, 2017

Abstract—Thermal reduction of graphite oxide and its derivatives under argon atmosphere has been studied by means of thermogravimetric analysis. Carbon materials prepared via thermal reduction of graphite oxide derivatives in argon at 900°C during 3 h have been used for deposition of platinum from H₂PtCl₆ solutions. Pt particles supported on the support catalyze liquid-phase hydrogenation of nitrobenzene and dec-1-ene under atmospheric pressure of H₂. Thermal reduction of the supports based on graphite oxide results in the formation of the structural defects significantly enhancing the catalytic activity.

Keywords: graphite oxide, thermal reduction, platinum catalyst, liquid-phase hydrogenation, nitrobenzene, dec-1-ene

DOI: 10.1134/S1070363217070040

Carbon materials with graphene-like structure that contain a system of conjugated bonds capable of the substrate coordination and electron transfer [1] are interesting supports for fixation of catalysts and electrocatalysts. Conjugated *sp*²-hybrid graphene structure does not contain any functional groups. Therefore, strong bonds are not formed during deposition of a catalytically active metal on the support surface; this results in the lability of the supported metal, the particles aggregation, and decrease of catalytic activity. We have earlier demonstrated the possibility of platinum fixation on carbon nanotubes and nanofibers containing a small fraction on functional groups, to prepare active and stable hydrogenation catalysts [2, 3]. Graphene exhibits high theoretical specific surface area, high electroconductivity, and high mobility of charge carriers and room temperature; therefore, it can be a promising support [4] for the catalyst of reactions involving electron transfer. Graphite oxide containing numerous oxygen-containing groups prone to the formation of strong covalent bonds with metal ions is a common precursor for the graphene-like materials [5]. After deposition of the metal ions, the composition is reduced; however, the

*sp*²-hybrid structure of graphite layers cannot be reduced by chemical or thermal methods [6].

We have earlier prepared platinum-containing compositions via simultaneous reduction of graphite oxide and H₂PtCl₆ [7] and deposition of platinum from H₂PtCl₆ on chemically [8] and thermally [9] reduced graphite oxide. Such compositions have been tested as catalysts in model reactions of liquid-phase hydrogenation of nitrobenzene and dec-1-ene. The platinum-containing composition based on thermally reduced graphite oxide [9] are more active than those with chemically reduced graphite oxide [8] or prepared via simultaneous reduction [7].

Thermally reduced graphite oxide has been prepared in two stages, one of them (fast thermolysis of graphite oxide) is accompanied by explosion and is thus inconvenient. In this study, we investigated the possibility of using chemical reduction of graphite oxide instead of its fast thermolysis. In particular, we studied thermal reduction of graphite oxide as well as the products of its fast thermolysis and chemical reduction under argon atmosphere. Platinum-containing compositions were prepared based on the products

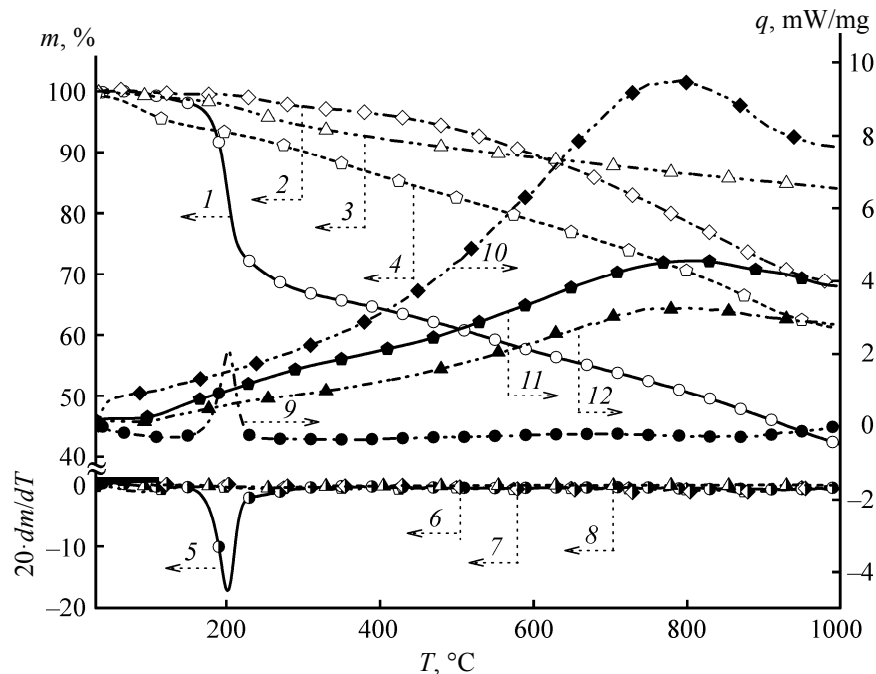


Fig. 1. Thermograms, integral curves, and DSC curves for graphite oxide at the heating rate 3 deg/min (1, 5, 9) and for the products of fast thermolysis of graphite oxide (2, 6, 10) and graphite oxide reduced by $\text{N}_2\text{H}_4\cdot\text{H}_2\text{O}$ (3, 7, 11) and NaBH_4 (4, 8, 12) at the heating rate 10 deg/min.

of the thermal reduction under argon at 900°C during 3 h, and their catalytic properties in model hydrogenation reactions were determined.

Thermal transformations of graphite oxide have been described in detail in the literature. However, the data is contradictory because graphite oxide is not an individual compound with a strictly defined structure. Fast heating of graphite oxide under argon to 1050°C has afforded a goffered carbon materials with the C/O molar ratio of about 10 [12]. Heating of graphite oxide to ~200°C leads to sharp mass decrease (the fast heating leads to explosion) [13, 14]. Thermal decomposition of graphite oxide accompanied by explosion has been observed at a lower temperature (127°C) as well [15]. It has been shown that carboxyl groups at the edges of the graphene layers of graphite oxide are readily decomposed at heating, whereas the carbonyl groups can be hardly removed [16]. The epoxy groups of graphite oxide react with adjacent hydroxyl groups at temperature >400°C and are transformed into the phenolic moieties, the latter dominating over the carbonyl ones even at temperature >1000°C. Thermal reduction of graphite oxide leads first to elimination of carboxyl, epoxy, and hydroxyl groups, whereas stable phenolic and carbonyl groups as well as fragments of cyclic ethers are retained up to high temperature (>800°C) [17].

It has been earlier observed [7, 9] that graphite oxide decomposes with explosion to evolve carbon oxides (CO and CO_2) and water during fast (~10 deg/min) heating to ~200°C. To determine the reduction temperature T_r and the activation energy E_a , we studied thermal reduction of graphite oxide at heating rates 1, 2, 3, and 4 deg/min (when the explosion did not occur) by means of thermogravimetric analysis. The specimen mass loss of ~60–65% was observed upon graphite oxide heating to 1000°C (Fig. 1, curve 1). In line with the data in [13, 14], the sharp mass loss (30–35%) was observed at ~190–215°C, accompanied by the exothermic effect (as seen in the DSC curve, Fig. 1, curves 1 and 9). Further mass loss occurred with constant rate (Fig. 1, curves 1 and 5). Temperature of thermal reduction of graphite oxide T_r in the DSC curve (Fig. 1, curve 9) coincided with the extremum in the integral TG curve (Fig. 1, curve 5). Likely, the formation of the product of fast thermolysis of graphite oxide accompanied the sharp mass loss with distinct exothermic effect at ~200°C.

It has been shown that a combination of chemical and thermal reduction allows more complete elimination of oxygen from graphite oxide [18]. For example, the reduction of graphite oxide with hydrazine eliminates the epoxy, hydroxyl, and carboxylic groups, whereas the carbonyl groups are only partially reduced

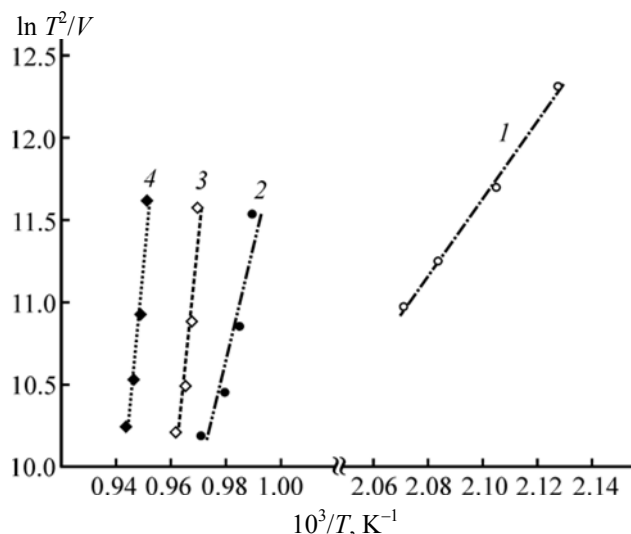


Fig. 2. Determination of activation energy of thermal reduction of graphite oxide (1), heat-expanded graphite oxide (2), and graphite oxide reduced by $N_2H_4 \cdot H_2O$ (3), and $NaBH_4$ (4) using the Kissinger equation.

by nitrogen addition. Carboxyl and epoxy groups of graphite oxide are thermally unstable, whereas the elimination of carbonyl groups and cyclic ether moieties requires high-temperature treatment. This means that the oxygen-containing groups retained after the reduction by N_2H_4 (carbonyl and cyclic ether ones) can be eliminated via high-temperature reduction [18].

In contrast to graphite oxide (Fig. 1, curves 1, 5, 9), thermal reduction of the products of its fast thermolysis (heat-expanded graphite oxide) or of chemical (with $N_2H_4 \cdot H_2O$ or $NaBH_4$) reduction occurred with constant rate (Fig. 1, curves 2–4, 6–8), close to that for graphite oxide after the extremum in curve 9, and was accompanied by broadened exothermic effect at higher temperature (Fig. 2, curves 10–12). Temperature of reduction T_r for heat-expanded graphite oxide and graphite oxide reduced by $N_2H_4 \cdot H_2O$ or $NaBH_4$ was determined from the maximum in the DSC curves at the heating rates 10, 20, 30, and 40 deg/min. Due to the broadening of the DSC curves for those samples, the determined T_r values were not very accurate and only reflected the general trend.

Effective activation energy of the thermal reduction E_a is related to the T_r value (K) and the heating rate v (deg/min) via the Kissinger equation (1) [19] that could be rewritten in the form (2).

$$\frac{E_a v}{k T_r^2} = A e^{E_a/k T_r}, \quad (1)$$

$$\ln A + \ln \frac{T_r^2}{v} = (E_a/R)(1/T_r), \quad (2)$$

where A is a pre-exponent factor and R is universal gas constant. Using the T_r values determined at different heating rates v , it is possible to determine the activation energy E_a from the $\ln T_r^2/v - (1/T_r)$ plot (Fig. 2) as the slope of the curve times R .

The data processing showed that graphite oxide is reduced at relatively low temperature (190–215°C) with the activation energy ~ 14 kJ/g, close to the values reported in [13, 19]. Of the graphite oxide derivatives, the sample treated with hydrazine hydrate was reduced most readily, with the activation energy ~ 46 kJ/g. Graphite oxide reduced by $NaBH_4$ and heat-expanded graphite oxide showed higher activation energies, of ~ 54 and ~ 60 kJ/g, respectively. Since temperature of reduction T_r of the chemically reduced and heat-expanded graphite oxide did not exceed 800°C (according to the TGA data, Fig. 1), their thermal reduction was performed at 900°C.

Oxygen content in the samples prepared via thermal reduction of the products of chemical reduction of graphite oxide with $N_2H_4 \cdot H_2O$ (1) and $NaBH_4$ (2) was significantly lower than that in the sample prepared via thermal treatment of heat-expanded graphite oxide (3) (see the table), i.e., combined chemical and thermal reduction of graphite oxide led to more complete elimination of oxygen than fast thermolysis followed by thermal reduction.

IR spectra of samples 1–3 (Fig. 3, curves 1, 3, 5) were smoother in comparison with the starting graphite oxide [8, 9]. The absorption bands of the alkoxy groups (C–O stretching at 1065 cm^{-1}) were substituted with the bands of phenolic (1100 cm^{-1}) and C–OH (1165 and 1215 cm^{-1}) groups, and the bands of epoxides and cyclic ethers at 863 , 965 , and 1407 cm^{-1} became stronger. The absorption bands of the C–N groups (1460 cm^{-1}) were most noticeable in the spectrum of sample 1 prepared from graphite oxide reduced by hydrazine hydrate. Absorption band of the Ph–CO fragments (1620 cm^{-1}) were absent in the products of thermal reduction, whereas those of the carboxylic C=O groups (1726 cm^{-1}) were retained. Following the data in [20, 21], the band at 1566 cm^{-1} assigned to the deformation vibrations of the CH–CH fragments evidenced the restoration of the sp^2 -hybrid structure of graphite, but the presence of absorption bands of symmetric and asymmetric stretching of

Elemental analysis data and catalytic activity of the studied samples

Sample	Content, wt %					Formula	C/O molar	I_D/I_G	Specific activity in hydrogenation, (mol H ₂)(mol Pt) ⁻¹ min ⁻¹	
	C	H	N	O	Pt				nitrobenzene	dec-1-ene
Graphite oxide	49.31	2.42	0.03	45.02	–	C ₈ H _{4.68} O _{5.48}	1.46	1.52	–	–
1	92.55	0.11	2.11	0.90	–	C ₈ H _{0.11} N _{0.16} O _{0.06}	133.33	1.39	–	–
Pt/ 1	89.72	0.70	2.36	2.82	5.80	Pt/C ₈ H _{0.74} N _{0.18} O _{0.19}	42.105	1.53	50.7	60.1
2	90.38	0.12	0	4.055	–	C ₈ H _{0.13} O _{0.27}	26.63	1.62	–	–
Pt/ 2	89.45	0.12	0.29	3.25	5.77	Pt/C ₈ H _{0.13} N _{0.02} O _{0.22}	36.36	1.76	119.3	157.8
3	86.45	0.70	0	8.64	–	C ₈ H _{0.77} O _{0.60}	13.33	1.67	–	–
Pt/ 3	80.70	0.70	0.73	8.12	5.72	Pt/C ₈ H _{0.83} N _{0.06} O _{0.60}	13.33	1.79	150.8	318.2
Heat-expanded graphite oxide reduced at 1000°C (4)	91.9	1.0	0.54	2.8	–	C ₈ H _{1.04} N _{0.04} O _{0.18}	44.44	2.44	–	–
Pt/ 4	84.58	0.57	0.53	4.42	6.55	Pt/C ₈ H _{0.64} N _{0.04} O _{0.31}	25.81	2.02	322	153.6
Graphite oxide reduced by N ₂ H ₄ ·H ₂ O (5)	79.59	0.97	3.32	9.58	–	C ₈ H _{1.16} N _{0.29} O _{0.72}	1.065	1.59	–	–
Pt/ 5	78.68	0.594	2.77	9.07	5.875	Pt/C ₈ H _{0.72} N _{0.24} O _{0.69}	11.56	1.46	31.9	25.5
Graphite oxide reduced by NaBH ₄ (6)	76.63	0.74	0.03	13.87	–	C ₈ H _{0.92} O _{0.87}	7.36	1.73	–	–
Pt/ 6	74.74	0.96	0.21	15.24	6.525	Pt/C ₈ H _{1.22} N _{0.02} O _{1.22}	6.53	1.455	34.9	14.85
Heat-expanded graphite oxide (7)	76.17	1.33	0.45	19.39	–	C ₈ H _{1.66} O _{1.53}	5.23	1.76	–	–
Pt/ 7	69.97	1.66	0.30	19.135	6.69	Pt/C ₈ H _{2.26} N _{0.03} O _{1.75}	4.57	1.74	62.5	56.4
Heat-expanded graphite oxide reduced at 1050°C (8)	94.28	0.59	0.40	1.52	–	C ₈ H _{0.60} N _{0.03} O _{0.065}	123.08	1.50	–	–
Pt/ 8	86.48	0.79	0.77	4.29	6.53	Pt/C ₈ H _{0.87} N _{0.05} O _{0.3}	26.67	1.27	205	113.6
Pt/AP-B ^a	70.88	1.00	–	–	7.645				63.4	34.8

^a AP-B is activated recuperation carbon.

methyl and methylene groups (at 2853 and 2923 cm⁻¹) as well as those of the CH–CH fragments and oxygen-containing groups in the IR spectra contradicted the *sp*²-hybrid structure of graphite.

The observed IR spectra of the products of thermal reduction coincided with the conclusions of thermal

stability of phenols, cyclic ethers, and carbonyl groups [16–18].

Raman spectra of the samples **1–3** (Fig. 4), similarly to the spectra of the starting heat-expanded graphite oxide and graphite oxide reduced by N₂H₄·H₂O and NaBH₄, contained strong D- and G-maximums

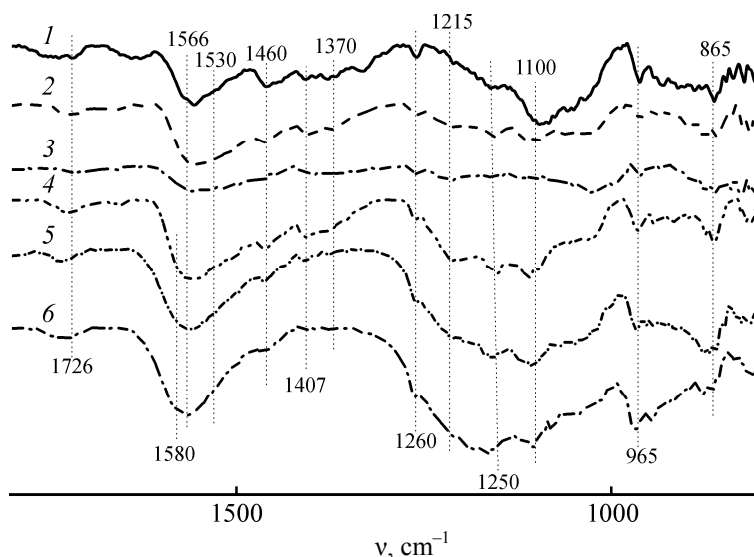


Fig. 3. IR spectra of the 1 (1), Pt/1 (2), 2 (3), Pt/2 (4), 3 (5), and Pt/3 (6) samples.

at 1344 and 1587 cm^{-1} , respectively. The ratio of integral intensities I_D/I_G reflecting the fraction of defects was slightly increased for the products of thermal reduction at 900°C (see the table). The second-order maximums at 2443, 2686, and 2918 cm^{-1} were broadened, evidencing the different number of the layers and deviation from the sp^2 -hybridization. Thermal reduction of heat-expanded graphite oxide at higher temperature (1000°C) resulted in the increased I_D/I_G ratio [9] (see the table), i.e. to the enhanced defectiveness. Hence, the defectiveness of the graphite oxide derivatives determined from the I_D/I_G ratio was governed by the fraction of the defects in the starting

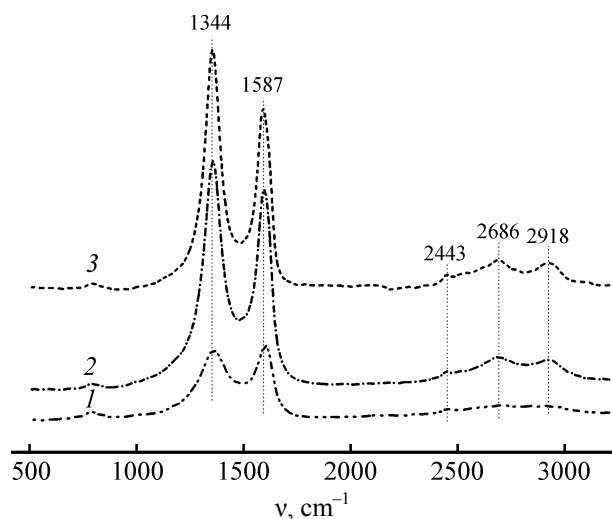


Fig. 4. Raman spectra of heat-expanded graphite oxide (1) and heat-expanded graphite oxide reduced by NaBH_4 (2), and $\text{N}_2\text{H}_4 \cdot \text{H}_2\text{O}$ (3).

graphite oxide and was increased upon its reduction (see the table). Our data on the effect of the procedure of graphite oxide reduction on the products defectiveness [7–9] agreed with the data of [6].

In the cases of platinum deposition on the starting graphite oxide via simultaneous reduction [7] and deposition of platinum on chemically reduced graphite oxide [8], the support is rich in oxygen-containing groups providing covalent binding of platinum with the carbon surface. For the supports with low oxygen content, covalent binding with a metal ion is hardly possible. It has been demonstrated theoretically and in the experiment that the energy of metal binding with oxidized graphene surface is much higher than for the non-oxidized surface [22]; in the absence of oxygen-containing groups, the metal ions are not supported on the carbon material surface [23]. Moreover, thermally or chemically reduced graphite oxide is prone to irreversible agglomeration [24] disfavoring metal ion coordination. At low content of oxygen groups at the support surface (as in [9], that was the case of samples 1–3), the functional groups required for platinum adsorption at the support could be introduced via noncovalent modification. In this work, we achieved that by adsorption of platinum and the following reduction performed in the presence of pyridine adsorbed at the graphite surface [25] and on graphene [26] via the π -complexes formation. Besides neutralization of H_2PtCl_6 and transformation of the latter in the cationic complex $\text{Pt}(\text{Py})_2\text{Cl}_4$, pyridine afforded the basic medium with the formation of pyridinium forms

that, like ionic liquids [27, 28] often used for metals deposition [29, 30], can be adsorbed on carbon materials. Those factors positively affected platinum deposition. For example, in contrast to the anionic complex of Pt(IV), reduction of the cationic complex with NaBH_4 yields small (≤ 1.7 nm) Pt clusters uniformly distributed over the support surface [31].

The amount of platinum supported on the samples 1–3 using the procedure elaborated elsewhere [7–9] corresponded to the theoretical one (see the table); the particles size estimated by TEM did not exceed 2 nm (Fig. 5). Different contrast of the Pt particles (Fig. 5) confirmed the layered structure of the defective support retained upon platinum deposition.

Deposition of Pt on the samples 1–3 was reflected in the IR spectra: the absorption bands of hydroxyl groups were strengthened and shifted to 1260 cm^{-1} , that effect was the most prominent for the Pt/3 sample (Fig. 3, curves 2, 4, 6). The observed broadening of the band of the hydroxyl groups evidenced the interaction of Pt clusters with phenolic hydroxyl groups present at the carbon material surface. The band of deformation vibrations of the CH–CH fragments (1566 cm^{-1}) in the spectrum of the Pt/3 sample was noticeably broadened (likely, due to the shift of the skeletal vibrations of the aromatic ring to 1530 and 1580 cm^{-1} induced by its conjugation with the lone electrons of Pt clusters) (Fig. 3, curves 5, 6). Such broadening was observed in the case of platinum deposition on graphite oxide thermally reduced at 1000 or 1050°C [9]. The spectra of the samples after platinum deposition assisted by pyridine contained the absorption bands of the C–N groups (1460 cm^{-1}) and the O–H groups of intercalated water (1370 cm^{-1}) (Fig. 3, curves 2, 4, 6).

Position of the first-order maximums (1344 and 1587 cm^{-1}) in the Raman spectra of the samples 1–3 was not affected by deposition of platinum on their surface. The maximum at 2443 cm^{-1} assigned, in our opinion, with the presence of the sp^3 -hybridized amorphous carbon was distinct in the spectrum of the Pt/1 system (Fig. 6). As in the case of thermal reduction (Fig. 4), the 2D maximum at 2710 cm^{-1} typical of graphite and graphene [32] was absent in the spectra of the Pt/1, Pt/3, and Pt/2 samples, evidencing the higher defectiveness of the samples and insignificant amount of graphene domains in their structure.

The prepared Pt-containing compositions catalyzed liquid-phase hydrogenation of nitrobenzene to aniline (Fig. 7). The Pt/2 and Pt/3 samples supported

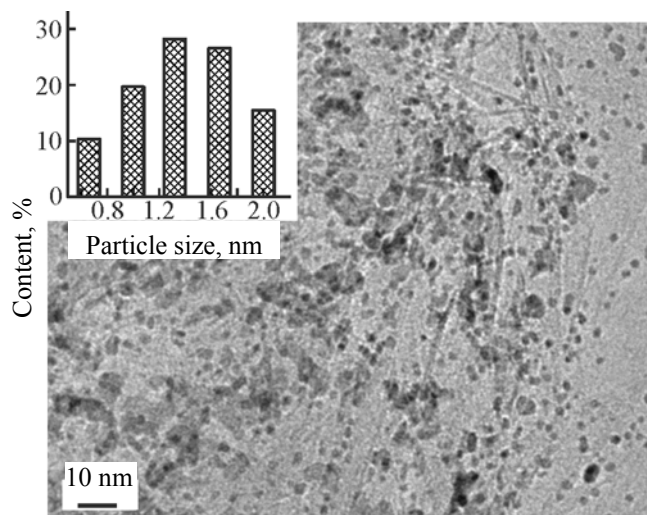


Fig. 5. TEM image of the Pt/1 sample. The inset shown the histogram of the Pt particles size distribution.

on thermally reduced samples of graphite oxide pretreated with NaBH_4 and heat-expanded graphite oxide (Fig. 7, curves 5, 6) were more active than the Pt compositions based on the same graphite oxide samples not subject to thermal reduction (Fig. 7, curves 2, 4). The Pt/1 sample was more active than the Pt/5 one, the latter being based on graphite oxide reduced by hydrazine hydrate (Fig. 7, curve 3), but was noticeably less active than the samples based on graphite oxide reduced by NaBH_4 (Pt/6) and heat-expanded graphite oxide (Pt/7). As has been shown in this and earlier studies [7, 8], activity of platinum catalysts supported on graphite oxide-based supports containing nitrogen after the reduction by $\text{N}_2\text{H}_4 \cdot \text{H}_2\text{O}$ in hydrogenation of nitrobenzene is much less than for the supports prepared via reduction by NaBH_4 or fast thermolysis. The similar trend has been observed for platinum catalysts on nanotubes or graphite oxide reduced by $\text{N}_2\text{H}_4 \cdot \text{H}_2\text{O}$ [33]. The incorporation of nitrogen in the graphene-like structure (3.5% in this work) observed upon reduction of graphene oxide with hydrazine hydrate leads to the increased positive charge of the carbon surface of the support [34]. As marked in [35, 36], this should facilitate the (electro)-oxidation processes demanding the positively charged material of the electrode or the catalyst and the basic reaction medium [37]. The basic reaction medium inhibits the hydrogenation due to the lack of protons [38]. The Pt/4 sample supported on the heat-expanded graphite oxide (Fig. 7, curve 7) and thermally reduced at 1000°C [8] was more active (see the table) than the Pt/3 sample supported on heat-expanded graphite

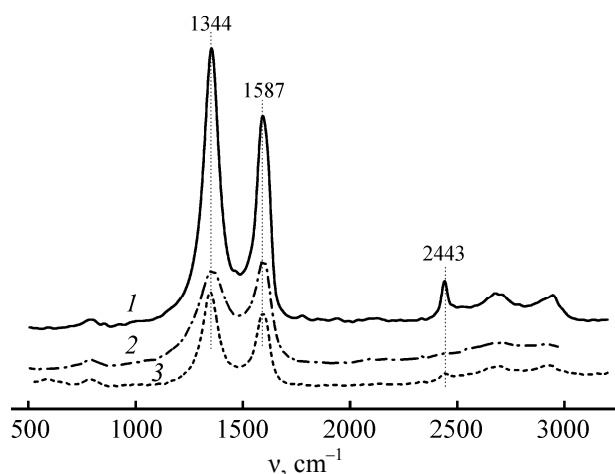


Fig. 6. Raman spectra of the Pt/1 (1), Pt/3 (2), and Pt/2 (3) samples.

oxide thermally reduced at 900°C. The deposited platinum was retained on the carbon surface during liquid-phase hydrogenation, and the prepared catalysts were highly stable even in the hydrogenation process with accumulation of the product (aniline) [8, 9].

The prepared compositions catalyzed liquid-phase hydrogenation of dec-1-ene into decane in propan-2-ol as well. The Pt/1, Pt/2, and Pt/3 catalysts supported on the supports thermally reduced at 900°C (Fig. 8, curves 4, 5, 7) were significantly more active than the catalysts based on heat-expanded graphite oxide (Pt/7) and graphite oxide reduced by NaBH₄ (Pt/6) and hydrazine hydrate (Pt/5) (Fig. 8, curves 1–3), the Pt/2 sample being close in the activity to Pt composition based on heat-expanded graphite thermally reduced at 1000°C, and the Pt/3 sample being more active than the latter.

The catalyst prepared via conventional deposition of platinum on the recuperation activated carbon AP-B (Pt/AP-B) was close in the activity to the Pt composition based on heat-expanded graphite oxide and evidently was less active than the Pt/3 sample (see the table).

Several examples of hydrogenation catalyst based on thermally reduced graphite oxide have been reported. Ruthenium, rhodium, and iridium supported on graphite oxide thermally reduced at 500–560°C via

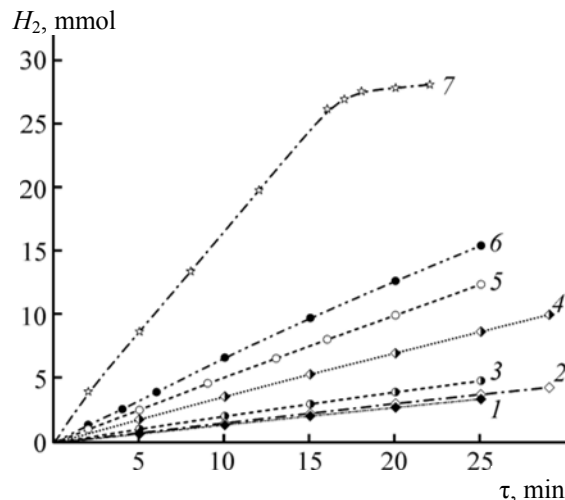


Fig. 7. Fragments of hydrogen uptake curves during hydrogenation of nitrobenzene in the presence of Pt compositions based on graphite oxide reduced by N₂H₄·H₂O (1) and NaBH₄ (2), heat-expanded graphite oxide (4), the Pt/1 (3), Pt/2 (5), Pt/3 (6), and Pt/4 (7) samples. The catalysts contained 0.867 mg (4.44×10⁻⁶ mol) of platinum.

decomposition of neutral carbonyls in the medium of ionic liquids or propylene carbonate catalyze hydrogenation of benzene and cyclohexene in bulk at temperature up to 100°C and H₂ pressure up to 10 bar, whereas the carbonyl complexes are not active [39–41]. Activity of these catalysts in hydrogenation of cyclohexene is moderate, accounting for the experiment conditions.

Hence, the TGA investigation revealed that graphite oxide was decomposed on heating under inert. At temperature ~200°C, sharp exothermic reaction accompanied by the mass loss due to evolution of water and carbon oxides was observed, further heating resulting in the linear mass loss. Thermal reduction of graphite oxide showed the activation energy of ~14 kJ/g. The products of chemical reduction or fast thermolysis of graphite oxide were not reduced so readily, and the corresponding activation energy was higher.

Thermal reduction of oxide graphite and its derivatives resulted in noticeable decrease in the oxygen content, but phenolic, carbonyl, and cyclic ether groups were retained. Defectiveness of the graphite oxide derivatives was determined by that of the starting material and was increased upon reduction.

Thermal reduction of the graphite oxide-based supports under argon at 900°C enhanced the activity of platinum particles supported on their surface in model

reactions of liquid-phase hydrogenation of nitrobenzene and dec-1-ene. The platinum catalyst deposited on heat-expanded graphite oxide (even before the thermal reduction) was more active than the catalysts based on chemically reduced samples (see the table). Hence, fast thermolysis of graphite oxide could not be replaced with its chemical reduction without the activity loss. The increase in temperature of thermal reduction of the product of fast thermolysis to 1000°C [9] significantly improved the activity of the deposited platinum particles. Nitrogen-containing graphite oxide reduced by hydrazine hydrate was not suitable as support of platinum catalyst hydrogenation, irrespectively of the treatment.

Activity of the catalysts supported on graphite oxide was independent on the oxygen content in the latter but changed with the I_D/I_G ratio. The defectiveness reflected by the I_D/I_G ratio was increased upon thermal reduction, especially at 1000°C (see the table). The presence of defects in the material increases its surface area, facilitates the metal deposition, and favored the adsorption of hydrogen as well as substrate (like nitrobenzene or dec-1-ene) on the hydrogenation catalyst. Tuning the defectiveness of carbon supports is a critical issue in the preparation of hydrogenation catalysts.

EXPERIMENTAL

Graphite oxide was prepared following the procedure in [10] adopted from a known method [11]. Reduction of graphite oxide with sodium borohydride and hydrazine hydrate was performed as described in [8]. Heat-expanded graphite oxide was prepared via fast thermolysis [9].

Thermal reduction of graphite oxide pretreated with $N_2H_4 \cdot H_2O$ and $NaBH_4$ as well as heat-expanded graphite oxide was performed in Ar flow at 900°C during 3 h [9], yielding samples 1–3, respectively.

Platinum-containing compositions were prepared as described elsewhere [8, 9].

The table lists the elemental analysis data, gross formulas (normalized to 8 carbon atoms for the ease of comparison with the reference data), and the C/O molar ratios.

Catalytic hydrogenation was performed in a constant-temperature vessel at vigorous shaking (600 min^{-1}), atmospheric pressure of hydrogen, and temperature 45°C. A weighed catalyst specimen (0.010–0.050 g) and 20 mL of propan-2-ol were put in the vessel and

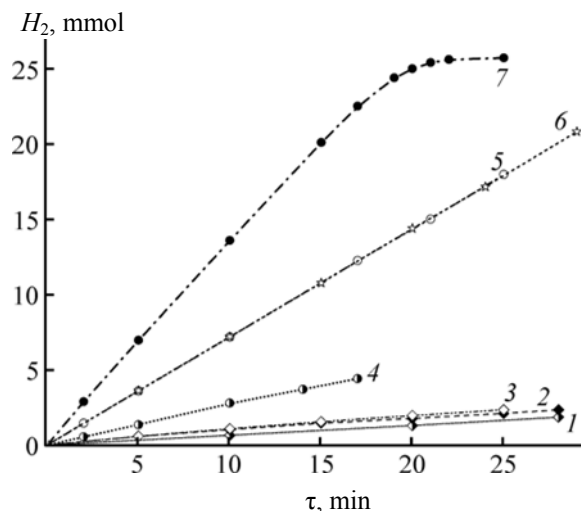


Fig. 8. Fragments of hydrogen uptake curves during hydrogenation of dec-1-ene in the presence of Pt compositions based on graphite oxide reduced by $NaBH_4$ (1) and $N_2H_4 \cdot H_2O$ (2), heat-expanded graphite oxide (3), the Pt/1 (4), Pt/2 (5), Pt/4 (6), and Pt/3 (7) samples. The catalysts contained 0.867 mg (4.44×10^{-6} mol) of platinum.

shaken under hydrogen during 0.5 h, 1 mL (1.199 g , $9.743 \times 10^{-3} \text{ mol}$) of nitrobenzene or 5 mL (3.704 g , $26.41 \times 10^{-3} \text{ mol}$) of dec-1-ene was then added, and the consumption of hydrogen was monitored by the volume measurement. The tabulated specific catalytic activity was calculated from the starting parts of the curves of hydrogen consumption (at the conversion below 5%).

Elemental analysis was performed using a Vario Micro cube CHNSO-analyzer (Elementar Analysensysteme GmbH, Germany). For the platinum-containing compositions, the contents of C and H were determined via the modified Pregl method, and Cl content was quantified via the Schoeniger method. The platinum content was determined from high-temperature residue mass via the Pregl method and additionally confirmed by means of energy-dispersive X-ray analysis. Thermogravimetry studies were performed using an STA-409 PC Luxx thermal analyzer combined with a QMS-403C mass spectrometer (NETZSCH, Germany). The specimens for TEM studies were prepared by dispersion of the powder in ethanol and applying onto a copper grid. The observation was performed using a JEM-2100 instrument (Center for Collective Usage, Scientific Center, Russian Academy of Sciences). The histogram of the particles size was plotted from TEM images by measuring the size of 200 particles. IR spectra were recorded over the $400\text{--}4000 \text{ cm}^{-1}$ using a Spectrum 100 spectrophotometer

(Perkin-Elmer, USA). Raman spectra were recorded using an RM1000 spectrometer (RENISHAW, Great Britain) equipped with a Leica microscope (20× magnification) at the excitation wavelength 532 nm (solid-state laser with diode pumping). The Raman spectra were fitted with the Lorentz peaks, and the integral intensities of the D- and G-maximums (I_D/I_G) were calculated as described elsewhere [8].

ACKNOWLEDGMENTS

The authors acknowledge L.N. Blinova (Institute of Problems of Chemical Physics, Russian Academy of Sciences) for thermogravimetric analysis.

This work was financially supported by the Russian Foundation for Basic Research (project 16-29-06197 ofi_m).

REFERENCES

1. Chepaikin, E.G. and Khidekel', M.L., *J. Mol. Catal.*, 1978, vol. 4, p. 103. doi 10.1016/0304-5102(78)80003-0
2. Kushch, S.D., Kuyunko, N.S., and Tarasov, B.P., *Kinet. Catal.*, 2009, vol. 50, no. 6, p. 860. doi 10.1134/s0023158409060093
3. Kushch, S.D., Kuyunko, N.S., and Tarasov, B.P., *Russ. J. Gen. Chem.*, 2009, vol. 79, no. 4, p. 706. doi 10.1134/s1070363209040057
4. Machado, B.F. and Serp, P., *Catal. Sci. Technol.*, 2012, vol. 2, no. 1, p. 54. doi 10.1039/c1cy00361e
5. Yu, J.-G., Yu, L.-Yan, Yang, H., Liu Qi, Chen, X.-H., Jiang, X.-Yu, Chen, X.-Q., and Jiao, F.-P., *Sci. Total Envir.*, 2015, vol. 502, p. 70. doi 10.1016/j.scitotenv.2014.08.077
6. Ju, H.-Mi, Huh, S.H., Choi, S.-Ho, and Le, H.-Lim., *Mater. Lett.*, 2010, vol. 64, no. 3, p. 357. doi 10.1016/j.matlet.2009.11.016
7. Kushch, S.D., Kuyunko, N.S., Muradian, V.E., and Tarasov, B.P., *Russ. J. Phys. Chem. (A)*, 2013, vol. 87, no. 11, p. 1798. doi 10.1134/s0036024413100117
8. Kushch, S.D., Kuyunko, N.S., Dremova, N.N., and Korshunova, L.A., *Kinet. Catal.*, 2015, vol. 56, no. 5, p. 584. doi 10.1134/s0023158415050110
9. Kushch, S.D., Kuyunko, N.S., Arbuzov, A.A., and Bondarenko, G.V., *Kinet. Catal.*, 2015, vol. 56, no. 6, p. 818. doi 10.1134/s0023158415060075
10. Arbuzov, A.A., Muradyan, V.E., and Tarasov, B.P., *Russ. Chem. Bull.*, 2013, vol. 62, no. 9, p. 1962. doi 10.1007/s11172-013-0284-x
11. Hummers, W.S., Jr. and Offeman, R.E., *J. Am. Chem. Soc.*, 1958, vol. 80, no. 6, p. 1339. doi 10.1021/ja01539a017
12. Schniepp, H.C., Li Je-L., McAllister, M.J., Sai, H., Herrera-Alonso, M., Adamson, D.H., Prud'homme, R.K., Car, R., Saville, D.A., and Aksay, I.A., *J. Phys. Chem. (B)*, 2006, vol. 110, no. 17, p. 8535. doi 10.1021/jp060936f
13. McAllister, M.J., Li Je-L., Adamson, D.H., Schniepp, H.C., Abdala, A.A., Liu, J., Herrera-Alonso, M., Milius, D.L., Car, R., Prud'homme, R.K., and Aksay, I.A., *Chem. Mater.*, 2007, vol. 19, no. 18, p. 4396. doi 10.1021/cm0630800
14. You Sh., Luzan, S.M., Szaby, T., and Talyzin, A.V., *Carbon*, 2013, vol. 52, p. 171. doi 10.1016/j.carbon.2012.09.018
15. Botas, C., Álvarez, P., Blanco, P., Santamaría, R., Granda, M., Gutiérrez, M.D., Rodríguez-Reinoso, F., and Menéndez, R., *Carbon*, 2013, vol. 52, p. 476. doi 10.1016/j.carbon.2012.09.059
16. Ganguly, A., Sharma, S., Papakonstantinou, P., and Hamilton, J., *J. Phys. Chem. (C)*, 2011, vol. 115, no. 34, p. 17009. doi 10.1021/jp203741y
17. Chen Ch.-M., Zhang, Q., Yang, M.-G., Huang Ch.-H., Yang, Y.-G., and Wang, M.-Zh., *Carbon*, 2012, vol. 50, no. 10, p. 3572. doi 10.1016/j.carbon.2012.03.029
18. Liang, X., Wang Yu, Zheng, H., and Wu, Z., *J. Electron Spectrosc.*, 2014, vol. 196, p. 89. doi 10.1016/j.elspec.2013.10.011
19. Yin, K., Li, H., Xia, Y., Bi, H., Sun, Jun, Liu, Zh., and Sun, L., *Nano-Micro Lett.*, 2011, vol. 3, no. 1, p. 51. doi 10.3786/nml.v3i1.p51-55
20. Song, P., Zhang, X., Sun, M., Cui, X., and Lin, Y., *RSC Adv.*, 2012, vol. 2, p. 1168. doi 10.1039/c1ra00934f
21. Teng, X., Yan, M., and Bi, H., *Spectrochim. Acta. (A)*, 2014, vol. 118, p. 1020. doi 10.1016/j.saa.2013.09.087
22. Prasomsri, T., Shi, D., and Resasco, D.E., *Chem. Phys. Lett.*, 2010, vol. 497, p. 103. doi 10.1016/j.cplett.2010.08.007
23. Goncalves, G., Marques, P.A.A.P., Granadeiro, C.M., Nogueira, H.I.S., Singh, M.K., and Grácio, J., *Chem. Mater.*, 2009, vol. 21, no. 20, p. 4796. doi 10.1021/cm901052s
24. Tung, T.Th., Feller, J.-F., Kim, T.Y., Kim, H., Yang, W.S., and Suh, K.S., *J. Polymer Sci. (A)*, 2012, vol. 50, no. 5, p. 927. doi 10.1002/pola.25847
25. Mohan, D., Singh, K.P., Sinha, S., and Gosh, D., *Carbon*, 2004, vol. 42, nos. 12–13, p. 2409. doi 10.1016/j.carbon.2004.04.026
26. Voloshina, E.N., Mollenhauer, D., Chiappisi, L., and Paulus, B., *Chem. Phys. Lett.*, 2010, vol. 510, nos. 4–6, p. 220. doi 10.1016/j.cplett.2011.05.025
27. Zheng, J.-N., He, Li-Li, Chen, Ch., Wang, Ai-Jun, Ma, Ke-Fu, and Feng, Jiu-Ju, *J. Power Sources*, 2014, vol. 268, p. 744. doi 10.1016/j.jpowsour.2014.06.109
28. Tong, Yu, Wang, Ch., Li, J., and Yang, Y., *Hydrometallurgy*, 2014, vols. 147–148, no. 6, p. 164. doi 10.1016/j.hydromet.2014.05.016
29. Crosthwaite, J.M., Muldoon, M.J., Dixon, J.K.,

- Anderson, J.L., and Brennecke, J.F., *J. Chem. Thermodyn.*, 2005, vol. 37, p. 559. doi 10.1016/j.jct.2005.03.013
30. Farooq, A., Reinert, L., Levkque, J.-M., Papaiconomou, N., Irfan, N., and Duclaux, L., *Micropor. Mesopor. Mater.*, 2012, vol. 158, p. 55. doi 10.1016/j.micromeso.2012.03.008
31. Amine Kh., Mizuhata, M., Oguro, K., and Takenaka, H., *J. Chem. Soc. Faraday Trans.*, 1995, vol. 91, no. 24, p. 4451. doi 10.1039/ft9959104451
32. Voiry, D., Yang, J., Kupferberg, J., Fullon, R., Lee, C., Jeong Hu, Y., Shin, H. Suk, and Chhowalla, M., *Nature*, 2016, vol. 353, no. 6306, p. 1413. doi 10.1126/science.aah3398
33. Nie, R., Wang, J., Wang, L., Qin Yu, Chen, P., and Hou, Zh., *Carbon*, 2012, vol. 50, no. 2, p. 586. doi 10.1016/j.carbon.2011.09.017.
34. Geng, D., Yang, S., Zhang, Y., Yang, J., Liu, J., Li, R., Sham, T.-K., Sun, X., Ye, S., and Knights, Sh., *Appl. Surface Sci.*, 2011, vol. 257, no. 21, p. 9193. doi 10.1016/j.apsusc.2011.05.131
35. Zhao, Y., Zhou, Y., O'Hayre, R., and Shao, Z., *J. Phys. Chem. Solids*, 2013, vol. 74, no. 11, p. 1608. doi 10.1016/j.jpcs.2013.06.004
36. Tang, Y., Yang, Z., and Dai, X., *Phys. Chem. Chem. Phys.*, 2012, vol. 14, no. 48, p. 16566. doi 10.1039/c2cp41441d
37. Bagotzky, V.S., Vassiliev, Yu.B., and Khazova, O.A., *J. Electroanal. Chem.*, 1977, vol. 81, no. 2, p. 229. doi 10.1016/s0022-0728(77)80019-3
38. Kushch, S.D., Izakovich, E.N., Khidekel', M.L., and Strelets, V.V., *Russ. Chem. Bull.*, 1981, vol. 30, no. 7, p. 1201. doi 10.1007/bf01417972
39. Marquardt, D., Vollmer Ch., Thomann, R., Steurer, P., Mülhaupt, R., Redel, E., and Janiak, Ch., *Carbon*, 2011, vol. 49, no. 4, p. 1326. doi 10.1016/j.carbon.2010.09.066
40. Esteban, R.M., Schütte, K., Brandt, Ph., Marquardt, D., Meyer, H., Beckert, F., Mülhaupt, R., Kölling, H., and Janiak, Ch., *Nano-Structures & Nano-Objects*, 2015, vol. 2, p. 11. doi 10.1016/j.nanoso.2015.07.001
41. Esteban, R.M., Schütte, K., Brandt, Ph., Marquardt, D., Barthel, J., Beckert, F., Mülhaupt, R., and Janiak, Ch., *Nano-Structures & Nano-Objects*, 2015, vol. 2, p. 28. doi 10.1016/j.nanoso.2015.07.002